

Hybrid Monte Carlo for Failure Probability Estimation with Gaussian Process Surrogates

Annie S. Booth* S. Ashwin Renganathan†

October 8, 2024

Abstract

We tackle the problem of quantifying failure probabilities for expensive computer experiments with stochastic inputs. The computational cost of evaluating the computer simulation prohibits direct Monte Carlo (MC) and necessitates a statistical surrogate model. Surrogate-informed importance sampling – which leverages the surrogate to identify suspected failures, fits a bias distribution to these locations, then calculates failure probabilities using a weighted average – is popular, but it is data hungry and can provide erroneous results when budgets are limited. Instead, we propose a hybrid MC scheme which first uses the uncertainty quantification (UQ) of a Gaussian process (GP) surrogate to identify areas of high classification uncertainty, then combines surrogate predictions in certain regions with true simulator evaluation in uncertain regions. We also develop a stopping criterion which informs the allocation of a fixed budget of simulator evaluations between surrogate training and failure probability estimation. Our method is agnostic to surrogate choice (as long as UQ is provided); we showcase functionality with both GPs and deep GPs. It is also agnostic to design choices; we deploy contour locating sequential designs throughout. With these tools, we are able to effectively estimate small failure probabilities with only hundreds of simulator evaluations. We validate our method on a variety of synthetic benchmarks before deploying it on an expensive computer experiment of fluid flow around an airfoil.

Keywords: computer experiment, deep Gaussian process, entropy, emulator, contour location, reliability, importance sampling

1 Introduction

Quantifying the probability of failure in complex dynamical systems is of great interest but is challenging due to the computational expense of the so-called “computer experiment.” Consider a black-box computer simulation, $f : \mathcal{X} \rightarrow \mathbb{R}$ with inputs $\mathcal{X} \subset \mathbb{R}^d$ governed by known measure $\mathbb{P}_{\mathbf{x}}$ (with density $p(\mathbf{x})$). The response is thresholded such that $f(\mathbf{x}) > t$ indicates failure. The research objective is to estimate the failure probability,

$$\alpha = \int \mathbb{I}_{\{f(\mathbf{x}) > t\}} d\mathbb{P}_{\mathbf{x}} = \int_{\mathbf{x} \in \mathcal{X}} \mathbb{I}_{\{f(\mathbf{x}) > t\}} p(\mathbf{x}) d\mathbf{x}. \quad (1)$$

We are particularly motivated by aeronautic applications where system failures may incur immense financial or environmental costs, or even loss of life. In aircraft design and development, computer simulation experiments are a natural, often mandatory, precursor to direct experimentation and deployment. For example, $f(\cdot)$ may represent the vibrations experienced by an aircraft which become unsafe above

*Corresponding author: Department of Statistics, NC State University, annie_booth@ncsu.edu

†Department of Aerospace Engineering, Penn State

certain levels, or the fuel efficiency of an aircraft, which if too low, can be detrimental to the environment, obliterate fuel budgets, or overly restrict travel distances. Inputs \mathcal{X} may encapsulate design parameters and operating conditions (such as wing shapes, aircraft design, flight speeds, and angles of attack). Yet we acknowledge a slew of other relevant applications where quantifying failure probabilities for complex simulations is critical, including structural reliability analysis using finite element simulations (e.g., [Mia et al., 2017](#)), Boltzmann modeling of chemical processes in fuel filtration (e.g., [Belot et al., 2021](#)), and thermodynamic flows for nuclear reactors (e.g., [Batet et al., 2014](#)).

A rudimentary approach to solve Eq. (1) involves brute force Monte Carlo (MC); simply sample an exhaustively large set of inputs, evaluate the computer simulation at each of these configurations, and report the proportion that resulted in failure. But this approach is prohibitively expensive if the computer simulation is costly (incurring long wall clock times), the probability of failure is rare (requiring enormous sample sizes), or both! In this work, we propose a novel method for quantifying failure probabilities of complex computer simulations when the computation budget restricts evaluations of the simulator to several hundred, rendering traditional MC impractical.

In the face of expensive data, statistical models (called “surrogates” or “emulators”) are essential. Surrogates are trained on a limited set of simulator evaluations in order to provide predictions with appropriate uncertainty quantification (UQ) at unobserved inputs. Gaussian processes (GPs) are the canonical choice ([Santner et al., 2003](#); [Gramacy, 2020](#)), but deep Gaussian processes (DGPs; [Damianou and Lawrence, 2013](#)) are becoming increasingly popular, particularly for non-stationary computer experiments ([Sauer, 2023](#)). Notably, our contribution is agnostic to surrogate choice as long as effective UQ is provided, and is thus applicable to traditional GPs and Bayesian DGPs ([Sauer et al., 2023b](#)) and, potentially, Bayesian neural networks ([MacKay, 1995](#)).

Early methods of failure probability estimation, namely the first and second order reliability methods (FORM/SORM; [Haldar and Mahadevan, 1995](#)), leveraged crude linear approximations of the complex model and placed all failure probability estimation in the hands of the “most probable point” on the predicted contour. Advancements on FORM and SORM have been made with more flexible GP models (e.g., [Su et al., 2017](#)). A variety of works have instead leveraged GP surrogates directly with MC sampling, using the GP predictions (which are of negligible cost) in place of true simulator evaluation (e.g., [Cheng and Lu, 2020](#); [Li et al., 2021](#); [Lu et al., 2023](#)). We will use this “surrogate MC” method as a benchmark in our later exercises. While it is cheap, it places too much stock in the accuracy of the surrogate and funnels surrogate inaccuracies directly into the failure probability estimate.

Importance sampling (IS; [Srinivasan, 2002](#); [Tokdar and Kass, 2010](#)) offers an unbiased alternative. It hinges on the construction of a bias distribution that intentionally focuses density in the failure region. Inputs are sampled from the bias distribution (hopefully yielding many failures) and are then utilized in a weighted average calculation that corrects for the disparity between the bias density and the original input density. Identifying an effective bias distribution in the face of limited training data is a hefty task ([Tabandeh et al., 2022](#)). Adaptive methods abound (e.g., [Oh and Berger, 1992](#); [Kurtz and Song, 2013](#); [Dalbey and Swiler, 2014](#); [Bugallo et al., 2017](#); [Cheng et al., 2023](#)). [Peherstorfer et al. \(2016\)](#) propose what they termed “multifidelity importance sampling,” although we prefer the term “surrogate-informed importance sampling” (SIIS) to avoid confusion with multifidelity surrogate modeling (e.g., [Park et al., 2017](#)). In SIIS, a surrogate is used to identify predicted failures, and a bias distribution is fit to these locations (more on this in Section 2.2). SIIS has been deployed with GP surrogates in a variety of subsequent works (e.g., [Cole et al., 2023](#); [Renganathan et al., 2023](#); [Booth et al., 2024a](#); [Renganathan, 2024](#)), and we view it as our primary competitor. Yet SIIS has several crucial drawbacks. We will delay a thorough discussion to Section 2.2, but the punchline is simply that IS has too much variability when bias distributions are suboptimal and data sizes are limited. The difficulty in training an effective bias distribution can render

SIIS estimated failure probabilities ineffective, forming the motivation behind our current contribution.

We argue that utility and precision in practice are more important than theoretical unbiasedness. To this end, we embrace a hybrid Monte Carlo calculation that uses both surrogate predictions and true simulator evaluations in strategically partitioned regions of the input space. [Li and Xiu \(2010\)](#) first proposed such a hybrid calculation, but their work was restricted to polynomial chaos (PC) models with strict accuracy assumptions in order to guarantee convergence. GP-based surrogates afford several key advancements over PCs. For one, GPs are flexible and data-driven; their accuracy continuously improves as training data sizes increase. Perhaps more importantly, GPs offer UQ through posterior variances. We leverage this UQ to prioritize expensive model evaluation at locations where the surrogate is least certain in its pass/fail prediction.

Regardless of how a surrogate is to be used (surrogate MC, SIIS, our hybrid MC, etc.), surrogate accuracy in identifying failure regions is of primary importance. Not all training designs are created equally. Space-filling designs ([Joseph, 2016](#)) may miss failure regions altogether, particularly when training budgets are limited. Instead, it is common to train a surrogate on a small initial design then pair it with a relevant acquisition function to select subsequent inputs for evaluation through the simulator. This iterative process of acquisition and surrogate updating can strategically hone in on the contour, all while minimizing evaluations of the expensive simulator. So-called “contour location” (CL) naturally outperforms space-filling counterparts. Acquisition functions seek to balance exploitation and exploration by leveraging both predicted distance from the contour and posterior uncertainty. Popular variations fall under expected improvement frameworks ([Bichon et al., 2008](#); [Ranjan et al., 2008](#)), stepwise uncertainty reduction frameworks ([Bect et al., 2012](#); [Chevalier et al., 2014](#); [Azzimonti et al., 2021](#)), or both ([Duhamel et al., 2023](#)). Others utilize pass/fail predictive entropy ([Marques et al., 2018](#); [Cole et al., 2023](#)). [Booth et al. \(2024b\)](#) recently extended CL sequential designs to DGP surrogates. We will utilize state-of-the-art sequentially designed GP and DGP surrogates in our benchmark exercises, but our contribution is agnostic to these choices. We see our method’s “plug-and-play” nature as a distinct advantage.

Both surrogate training and failure probability estimation require a budget of expensive simulator evaluations. These two tasks are typically conducted in independent stages, with separate pre-determined budgets (as we will use in the first round of our synthetic benchmarks). Yet, in practice, it is common for a total budget to be set according to computational allowances, with no mention of how many evaluations to spend on the training phase versus the estimation phase. Some works have investigated stopping criteria for surrogate training in reliability settings (e.g., [Echard et al., 2011](#); [Hristov et al., 2019](#)), but this is still an under-examined area of the literature. In our hybrid MC set-up, we have a unique advantage: the more we train our surrogate, the more certain it will be, requiring fewer high-cost evaluations for effective failure probability estimation. There is a clear give-and-take between the budgets of the training and estimation stages; increasing the budget of one decreases the budget required for the other, and vice versa. Leveraging this trade-off, we propose a method for allocating a fixed budget between surrogate training and hybrid Monte Carlo estimation.

This manuscript is laid out as follows. First, in [Section 2](#), we review GP/DGP surrogates and competing methods of failure probability estimation. In [Section 3](#) we present our proposed hybrid Monte Carlo procedure, including implementation details and a variety of synthetic benchmarking exercises. In [Section 4](#) we propose our budget allocation scheme, continuing the established benchmarks. Finally, we deploy our method on a computer experiment of an RAE-8288 airfoil in [Section 5](#) and conclude in [Section 6](#).

2 Failure probability estimation

Denote single inputs as the row vector \mathbf{x} of size $1 \times d$ with response $y = f(\mathbf{x})$. Let X_n represent the row-combined matrix of n -many inputs with corresponding response vector \mathbf{y}_n . Our objective is to quantify the failure probability from Eq. (1), namely $P(f(\mathbf{x}) > t)$ for $\mathbf{x} \sim p(\mathbf{x})$. Typical Monte Carlo with a budget of size M provides the estimator

$$\hat{\alpha}_{\text{MC}} = \frac{1}{M} \sum_{i=1}^M \mathbb{I}_{\{f(\mathbf{x}_i) > t\}} \quad \text{for } \mathbf{x}_i \stackrel{\text{iid}}{\sim} p(\mathbf{x}). \quad (2)$$

This estimator is ineffective unless a sufficient number of failures are observed, necessitating very large M particularly for small α . But our computer model $f(\mathbf{x})$ is expensive; we simply cannot evaluate it thousands/millions/billions of times. We will describe our sample efficient method for estimating failure probabilities in Section 3, after a quick review of preliminaries.

2.1 Gaussian process surrogates

A surrogate model \hat{f} , trained on a limited budget of runs, may provide predictions at unobserved inputs in place of the true f . To enable our proposed methodology the surrogate must also provide posterior predictive distributions. Gaussian processes (GPs) are the predominant choice; they assume a multivariate normal prior distribution over the response, $y \sim \mathcal{N}(\mu, \Sigma(X))$. The prior mean μ is often simplified to the zero vector (which we will use moving forward), and the prior covariance $\Sigma(X)$ is typically a function of inverse euclidean distances, e.g. $\Sigma(X)^{ij} = \Sigma(\mathbf{x}_i, \mathbf{x}_j) = k(\|\mathbf{x}_i - \mathbf{x}_j\|^2)$ with kernel $k(\cdot)$. See [Santner et al. \(2003\)](#); [Rasmussen et al. \(2006\)](#); [Gramacy \(2020\)](#) for thorough reviews. Conditioned on training data $\{X_n, \mathbf{y}_n\}$, posterior predictions at singleton input \mathbf{x} follow

$$\hat{f}_n(\mathbf{x}) \sim \mathcal{N}(\mu_n(\mathbf{x}), \sigma_n^2(\mathbf{x})) \quad \text{for} \quad \begin{aligned} \mu_n(\mathbf{x}) &= \Sigma(\mathbf{x}, X_n) \Sigma(X_n)^{-1} \mathbf{y}_n \\ \sigma_n^2(\mathbf{x}) &= \Sigma(\mathbf{x}) - \Sigma(\mathbf{x}, X_n) \Sigma(X_n)^{-1} \Sigma(X_n, \mathbf{x}), \end{aligned} \quad (3)$$

where $\Sigma(\mathbf{x}, X_n)$ denotes the vector formed from applying the kernel between \mathbf{x} and every row of X_n . Joint predictions are straightforward but not necessary for our contribution.

A natural alternative to true MC (Eq. 2) is ‘‘surrogate MC’’ which leverages surrogate predictions in place of the true simulator,

$$\hat{\alpha}_{\text{SURR}} = \frac{1}{M} \sum_{i=1}^M \mathbb{I}_{\{\mu_n(\mathbf{x}_i) > t\}} \quad \text{for } \mathbf{x}_i \sim p(\mathbf{x}). \quad (4)$$

If the surrogate is not accurate near the contour, it will misclassify inputs which will severely hinder the effectiveness of this estimator.

For example, consider the two-dimensional ‘‘Herbie’’ function ([Lee et al., 2011](#)) shown in the left and center panels of Figure 1 (we will revisit the right panel momentarily). We define a failure threshold of $t = 1.065$ which demarcates four disjoint failure regions (red contours). We also define $p(\mathbf{x})$ using independent normal distributions centered at the origin (solid black contours).¹ We trained a GP surrogate using a random Latin hypercube sample (LHS; [McKay et al., 2000](#)) of size $n = 100$ in the two dimensions. Figure 2 shows the GP posterior prediction along the slice $x_2 = 1.1$. The posterior mean (blue dashed) and 95% CI (blue shading) capture the true nonlinear surface (solid black) fairly well. Even so, there are inputs (highlighted by the yellow shading) which the surrogate would misclassify as ‘‘passes’’ instead of ‘‘failures.’’ Thus any estimate reliant solely on this surrogate would underestimate the failure probability.

¹Full details of all simulated functions, thresholds, and distributions are provided in the Supplementary Material.

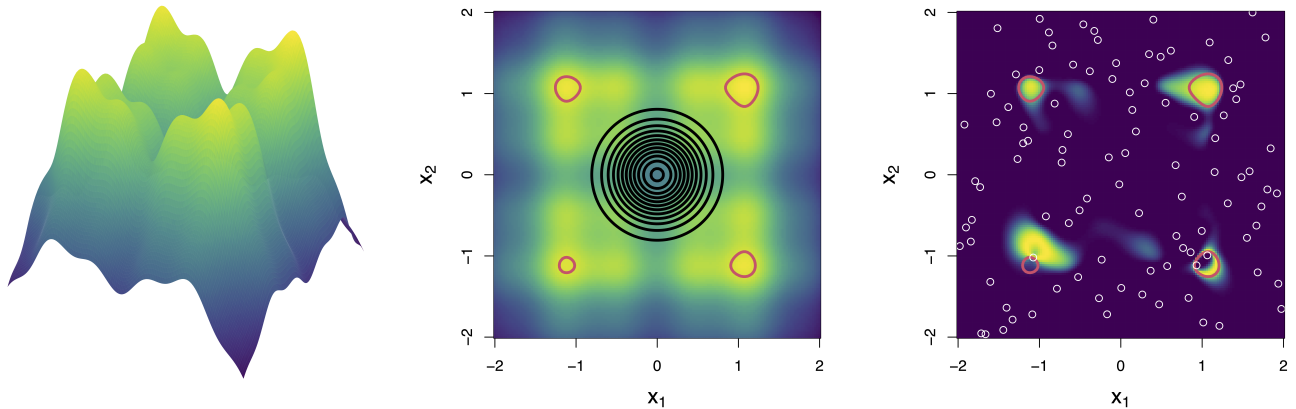


Figure 1: *Left/Center*: Herbie function with failure contour (red) and input distribution (black). *Right*: Entropy surface (yellow/high, purple/low) for a GP trained on a 100 point LHS (white circles).

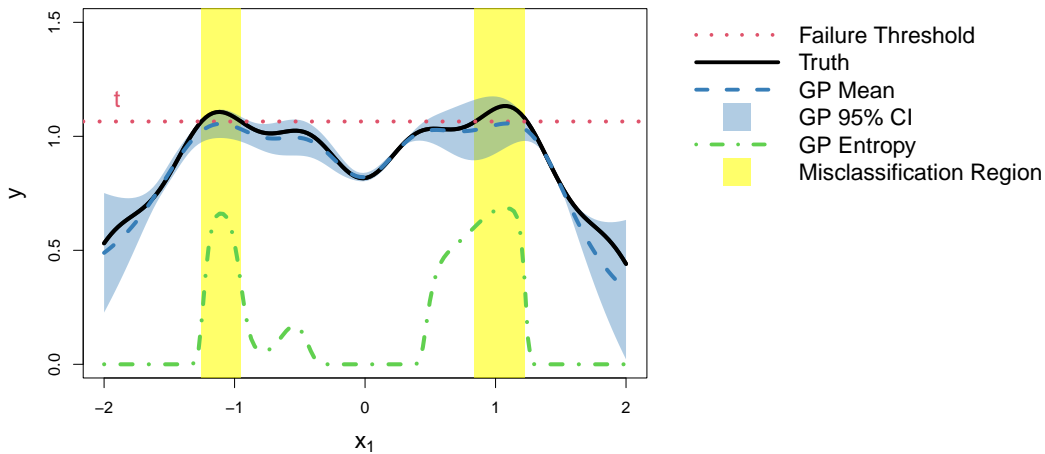


Figure 2: Slice of Herbie function along $x_2 = 1.1$. GP was trained on 100 point LHS in 2 dimensions.

Deep Gaussian processes. In some situations, surrogate predictions may be improved through adaptations to the surrogate model itself. Traditional GPs are limited by the commonly assumed stationarity of the covariance kernel; they are not able to accurately model non-stationary surfaces characterized by regime shifts and stark transitions. Deep Gaussian processes (Damianou and Lawrence, 2013) are a promising more flexible alternative. They leverage functional compositions of GP layers in which latent layers act as warped versions of the original inputs, allowing for greater flexibility. DGPs have consistently outperformed stationary GPs in modeling non-stationary computer experiments (e.g., Rajaram et al., 2021; Yazdi, 2022; Ming et al., 2023), particularly when deployed in a Bayesian framework with full UQ (e.g., Sauer et al., 2023b,a). See Sauer (2023) for a thorough review of DGP surrogates. Crucially, our method is agnostic to surrogate choice as long as UQ is provided. We will demonstrate functionality with both traditional GP and Bayesian DGP surrogates in Section 3.2.

Contour location. To facilitate failure probability estimation, a surrogate’s sole task is to accurately classify passes and failures. Strategic sequential designs targeting the failure contour, i.e., “contour lo-

ation,” will outperform space-filling counterparts in this regard. In CL, after initializing with a small space-filling design, subsequent training locations are selected iteratively through the optimization of an acquisition criterion. The computer simulation is evaluated at the selected input(s), the surrogate is updated, and the process is repeated until the budget is exhausted or a stopping criterion is met.

Identifying acquisition criteria which effectively target failure contours is a hot topic, particularly in conjunction with GP surrogates, (e.g., Bichon et al., 2008; Ranjan et al., 2008; Bect et al., 2012; Chevalier et al., 2014; Marques et al., 2018; Cole et al., 2023). Here, we highlight one in particular – classification entropy – defined as

$$H(\mathbf{x}) = -p_{\mathbf{x}} \log(p_{\mathbf{x}}) - (1 - p_{\mathbf{x}}) \log(1 - p_{\mathbf{x}}), \quad (5)$$

where $p_{\mathbf{x}}$ represents the probability of failure at input \mathbf{x} . With a GP surrogate, this probability boils down to a Gaussian CDF computation:

$$p_{\mathbf{x}} = \mathbb{P} \left(\hat{f}(\mathbf{x}) > t \right) = 1 - \Phi \left(\frac{t - \mu_n(\mathbf{x})}{\sigma_n(\mathbf{x})} \right).$$

Returning to the Herbie example, the entropy surface for the trained GP is shown in the right panel of Figure 1 and along the slice in Figure 2 (green dotted/dashed). Notice the high entropy regions mostly agree with the locations of the true failure contour (we could improve upon this with a CL design instead of an LHS). A reasonable acquisition could fall in any of these local optima. Booth et al. (2024b) extended these ideas, with some necessary adaptations, to enable contour location with Bayesian DGP surrogates. Henceforth, all GPs and DGPs we consider will be from sequential CL designs.

2.2 Importance sampling

Rather than side-stepping the prohibitive computation of Eq. (1) with surrogate evaluations, importance sampling (Tokdar and Kass, 2010) avoids expensive evaluations by sampling from a different distribution altogether. Let $q(\mathbf{x})$ denote a “bias” density which shares domain with $p(\mathbf{x})$. The failure probability α may be equivalently represented as

$$\alpha = \int_{\mathbf{x} \in \mathcal{X}} \mathbb{I}_{\{f(\mathbf{x}) > t\}} \frac{p(\mathbf{x})}{q(\mathbf{x})} q(\mathbf{x}) d\mathbf{x}.$$

Monte Carlo approximation of this integral provides the estimator

$$\hat{\alpha}_{\text{IS}} = \frac{1}{B} \sum_{i=1}^B w_i \mathbb{I}_{\{f(\mathbf{x}_i) > t\}} \quad \text{where} \quad w_i = \frac{p(\mathbf{x}_i)}{q(\mathbf{x}_i)} \quad \text{for} \quad \mathbf{x}_i \sim q(\mathbf{x}). \quad (6)$$

The “bias weights” w_i account for the difference between the input density and the bias density. This estimator is theoretically unbiased and requires a smaller budget of simulator evaluations ($B \ll M$) if the bias distribution appropriately covers and targets the failure region (Srinivasan, 2002). But estimation of an effective bias distribution is tricky. The ideal bias distribution is $q(\mathbf{x})^* = \frac{1}{\alpha} \mathbb{I}_{\{f(\mathbf{x}) > t\}} p(\mathbf{x})$, but naturally neither α nor the indicator function are known *a priori*. For the sake of feasibility, $q(\mathbf{x})$ is traditionally constrained to a known distributional family, such as a Gaussian mixture model (GMM; Reynolds et al., 2009). Bias distribution training is then relegated to learning distributional parameters (in a GMM, these include the number of mixtures, mixture weights, and component means and variances), often accomplished through cross validation or information criteria maximization.

In “surrogate-informed importance sampling,” Peherstorfer et al. (2016) leverage a surrogate to identify predicted failures from a large sample of the input distribution, then train a GMM bias distribution to

these predicted failures. If the surrogate effectively identifies the failure region, then these samples should mimic the ideal $q(\mathbf{x})^*$. With a trained bias distribution in-hand, samples may be drawn from $q(\mathbf{x})$ and deployed in Eq. (6) to provide an estimate of the failure probability.

While SIIS has been widely embraced for its unbiasedness, it has several key weaknesses. First, the bias distribution, which features heavily in the final estimate of Eq. (6), is a completely auxiliary quantity. Hypothetically, two different bias distributions could produce the same samples $\{\mathbf{x}_i\}_{i=1}^B$, thus producing the same $\{f(\mathbf{x}_i)\}_{i=1}^B$. But in the calculation of Eq. (6), these two bias distributions would contribute different weights, resulting in different final answers even though the training data from the computer simulator was exactly the same. O’Hagan (1987) first pointed out this conundrum as a violation of the “Likelihood principle.” A second weakness is the restriction of $q(\mathbf{x})$ to distributional families like GMMs. Failure regions may be complex and may not fit nicely under these target distributions. Consequently, SIIS typically requires large B in order to adequately cover the failure region. For context, Peherstorfer et al. (2016) entertained $B \in \{100, 1000, 10000, 100000\}$ and found performance continued to improve as B increased. Furthermore, there is no clear avenue for determining the budget allocation between surrogate training and importance sampling estimation. Finally, the SIIS method does not leverage the full potential of the surrogate model. Many expensive simulator evaluations go into training the surrogate, and in the end the surrogate is only used to identify predicted failures, with no mention of its UQ. We suspect this is a byproduct of Peherstorfer et al. using reduced order models, which do not provide the UQ of a GP, in their seminal work. Ultimately, we propose a flexible estimation procedure which avoids bias distributions altogether, leverages surrogate UQ, and enables strategic budget allocation.

3 Hybrid Monte Carlo with GPs

In this section, we introduce a failure probability estimation scheme which (i) relies only on the surrogate model and the simulator data, (ii) leverages surrogate UQ in the estimation phase, and (iii) can provide effective estimates with a budget of only several hundred. Specifically, we will upgrade the Monte Carlo estimate of Eq. (2) so it requires fewer evaluations of $f(\mathbf{x})$ with minimal reduction in accuracy.

Our approach (and those of our competitors) may be organized into two sequential phases: the training of the surrogate and the estimation of the failure probability. Let N denote the number of simulator evaluations used to train the surrogate, and let B denote the remaining budget of simulator evaluations available for estimation. For the duration of this section, we assume both N and B are pre-determined; in Section 4 we will consider how to allocate evaluations between them. Recall, we are targeting expensive simulations where the total budget, $N + B$, is constrained to be in the hundreds.

3.1 Methodology

Let $\mathcal{U} \subset \mathcal{X}$ represent some subset of the input domain (boundary inclusive). We may partition the integral of Eq. (1) into two components as follows, with the corresponding Monte Carlo estimate,

$$\begin{aligned} \alpha &= \int_{\mathcal{U}} \mathbb{I}_{\{f(\mathbf{x}) > t\}} p(\mathbf{x}) d\mathbf{x} + \int_{\mathcal{X} \setminus \mathcal{U}} \mathbb{I}_{\{f(\mathbf{x}) > t\}} p(\mathbf{x}) d\mathbf{x} \\ &\approx \frac{1}{M} \left[\sum_{\mathbf{x}_i \in \mathcal{U}} \mathbb{I}_{\{f(\mathbf{x}_i) > t\}} + \sum_{\mathbf{x}_i \notin \mathcal{U}} \mathbb{I}_{\{f(\mathbf{x}_i) > t\}} \right] \quad \text{for } \mathbf{x}_i \stackrel{\text{iid}}{\sim} p(\mathbf{x}), \quad i = 1, \dots, M. \end{aligned}$$

Now, replace expensive evaluation of $f(\mathbf{x}_i)$ outside of \mathcal{U} with the surrogate prediction $\mu_N(\mathbf{x}_i)$, resulting in the following “hybrid Monte Carlo” estimator:

$$\hat{\alpha}_{\text{HYB}} = \frac{1}{M} \left[\sum_{\mathbf{x}_i \in \mathcal{U}} \mathbb{I}_{\{f(\mathbf{x}_i) > t\}} + \sum_{\mathbf{x}_i \notin \mathcal{U}} \mathbb{I}_{\{\mu_N(\mathbf{x}_i) > t\}} \right] \quad \text{for } \mathbf{x}_i \stackrel{\text{iid}}{\sim} p(\mathbf{x}), \quad i = 1, \dots, M. \quad (7)$$

The hybrid nature of this estimator is in the use of both true simulator evaluations (left term) and surrogate evaluations (right term). Each \mathbf{x}_i will fall under either the left indicator term or the right one, never both. The computational cost of this estimator is greatly reduced since evaluations of the surrogate are effectively free. The accuracy of this estimator is contingent upon the classification accuracy of the surrogate and the choice of \mathcal{U} . Here, we focus on the choice of \mathcal{U} , presuming we already have a trained GP-based surrogate in-hand. [Training a surrogate for contour location has been previously investigated, as we reviewed in Section 2.1.]

Rather than thinking of \mathcal{U} as a continuum, we find it easier to conceptualize our contribution with a discrete set of samples, which form the basis of any Monte Carlo estimator. Let X_M denote the row-combined matrix of M -many samples from $p(\mathbf{x})$. To deploy our estimator $\hat{\alpha}_{\text{HYB}}$, we need a decision rule for classifying each \mathbf{x}_i into or out of \mathcal{U} . In a perfect world, \mathcal{U} would capture all the samples which the surrogate would misclassify. We are not privy to this information, but we can leverage the surrogate’s UQ to identify the samples at which it is most uncertain. Recall, entropy (Eq. 5) quantifies the degree of uncertainty in the pass/fail prediction of a surrogate. Accordingly, our decision rule is strikingly simple – place the B -many samples from X_M with the highest entropy into \mathcal{U} . Denote these as $X_M^{\mathcal{U}}$. Hopefully our choice of the letter \mathcal{U} is now apparent - it denotes the inputs with the highest “**U**ncertainty”. Revisiting Figure 2, notice the high entropy regions (green dotted/dashed) align well with the misclassification regions (yellow). The entropy criterion is effectively identifying regions of high classification uncertainty where we could most utilize expensive true simulator evaluations.

Li and Xiu (2010) employed a hybrid estimator similar to that of Eq. (7), but they chose to allocate expensive simulator evaluations to samples predicted to be closest to the contour. We suspect this choice was motivated by their use of polynomial chaos expansion models as surrogates which do not facilitate UQ. Nevertheless, we will implement this allocation scheme with our hybrid Monte Carlo estimator as a competitor in our benchmark exercises later.

For a fixed N , B , and M , our method proceeds as follows. First, train the surrogate using N -many evaluations of the high fidelity simulator. Our method is agnostic to surrogate and design choice as long as the surrogate provides posterior predictive distributions for the calculation of entropy, but we prefer contour locating designs with GP or DGP surrogates. Second, sample a very large number of points $X_M \sim p(\mathbf{x})$ and use the surrogate to calculate the classification entropy for each sample following Eq. (5). Third, identify the B -many points in X_M with the highest entropy and evaluate the simulator at these locations. Fourth, update the surrogate with these new observations of the simulator. Finally, estimate $\hat{\alpha}_{\text{HYB}}$ following Eq. (7) by combining the simulator evaluations at $X_M^{\mathcal{U}}$ with surrogate predictions at all other samples of X_M .

This fourth step – updating the surrogate given the simulator data at the high-entropy sampled locations – is significant. In the end, the surrogate is trained on $N+B$ observations, making full use of all the available data. Since the $X_M^{\mathcal{U}}$ points are likely near a failure contour, they could significantly improve the accuracy of the surrogate near the contour. The ability to update the surrogate and make full use of all simulator data is a unique advantage over SIIS, whose final estimate is contingent only upon the B -many points sampled from the bias distribution.

There are some noteworthy distinctions between the training and estimation phases of our method. The N points used to initially train the surrogate are acquired anywhere in the domain \mathcal{X} , and assuming

they stem from a contour locating design, they seek to balance both exploration of the response surface and exploitation of the suspected contour. In fact, the contour locating sequential design strategies we will use next (Cole et al., 2023; Booth et al., 2024b) intentionally circumvent acquisitions based on maximal entropy in order to avoid clustered acquisitions and to promote more exploration of the surface. Alternatively, the B points used for the hybridization and final surrogate update must originate from $p(\mathbf{x})$, and they are solely exploitative. By nature, they will be clustered around the predicted contour. We contend that having a mix of data from these two realms is superior to either extreme. To demonstrate superiority over the first extreme, in which the entire budget is relegated to training the surrogate over \mathcal{X} ignorant of $p(\mathbf{x})$, we will offer empirical comparisons in our simulated examples. To justify this claim over the second extreme, in which all training data must stem from $p(\mathbf{x})$, we revisit the Herbie example of Figure 1. With the input distribution centered at the origin, the probability of generating any samples outside $[-1, 1]^2$ is very low. But a GP surrogate would benefit from some ‘‘anchor points’’ in these outer regions (Gramacy and Apley, 2015). This distinction will be less prominent if $p(\mathbf{x})$ is uniformly distributed over \mathcal{X} , but the trade-off between exploring in the training phase and exploiting in the estimation phase will still be impactful.

Choosing M . Larger M will produce more effective sum approximations of the true integrals, but we need surrogate predictions (e.g., Eq. 3) for every sample in X_M . Although this computation is significantly cheaper than evaluation of the expensive simulator, it may still be significant for large M , particularly with a heftier surrogate like a Bayesian DGP. Simply put, we would like M to be large enough without being too cumbersome.

To reason through this choice, let’s revisit the unbiased Monte Carlo estimate of Eq. (2). Notice the indicator $\mathbb{I}_{\{f(\mathbf{x}) > t\}}$ is a Bernoulli random variable with expected value α and variance $\alpha(1 - \alpha)$. Thus, the MC estimator has variance inversely proportional to M :

$$\mathbb{V}[\hat{\alpha}_{\text{MC}}] = \frac{1}{M^2} \sum_{i=1}^M \mathbb{V}[\mathbb{I}_{\{f(\mathbf{x}) > t\}}] = \frac{\alpha(1 - \alpha)}{M}.$$

Let $\sigma_\alpha = \sqrt{\frac{\alpha(1-\alpha)}{M}}$ denote the standard error of this estimator. If we knew α , we could determine M by thresholding this standard error. For example, to achieve a standard error less than 10% of α requires:

$$\sigma_\alpha < \frac{\alpha}{10} \quad \longrightarrow \quad \frac{100(1 - \alpha)}{\alpha} < M.$$

To achieve this precision, $\alpha = 10^{-4}$ requires M nearly 1 million, $\alpha = 10^{-5}$ requires M nearly 10 million, and $\alpha = 10^{-6}$ requires M nearly 100 million.

In reality, when the true α is unknown, we recommend either choosing M conservatively given expert insight into the anticipated failure probability or performing a pilot study where M is incremented say by one million at a time. Surrogate predictions are gathered along this incremental process, with α estimated along the way to inform the selection of M .

3.2 Synthetic experiments

In this section we provide a variety of synthetic experiments in which the training and estimation budgets, N and B respectively, are pre-determined. We start with three functions: the 2d Herbie function (Lee et al., 2011) with a total budget of 160, the 3d Ishigami function (Ishigami and Homma, 1990) with a total budget of 400, and the 6d Hartmann function (Picheny et al., 2013) with a total budget of 800. We split the total budget of evaluations evenly between training and estimation. Table 1 summarizes

these settings, among others. Functions are observed without noise to mimic a deterministic computer simulation. We define failure thresholds and input distributions for each function, resulting in the failure probabilities reported in Table 1. We choose M based on these α values to keep σ_α conservatively under 5%. All input distributions are variations/combinations of independent uniform and truncated normal distributions; further details of the functions, thresholds, and distributions are reserved for Supplementary Material.

Function	True α	Surrogate	d	n_0	N	B	M
Herbie	7.533×10^{-5}	GP	2	20	80	80	3.5×10^7
Ishigami	1.904×10^{-4}	GP	3	50	200	200	1.5×10^7
Hartmann	1.001×10^{-5}	GP	6	100	400	400	1.0×10^8
Plateau	8.530×10^{-4}	DGP	4	30	120	120	3.5×10^7

Table 1: Simulaton settings. True α values are estimated from 10 billion samples.

We begin with a random Latin hypercube sample (McKay et al., 2000) of size n_0 (chosen to be 25% of the total training budget, see Table 1). We train a GP surrogate using the `Scikit-learn` package in python (Pedregosa et al., 2011). We then conduct a sequential design following the entropy contour location scheme of Cole et al. (2023), until we reach a final design of size N . Ultimately, we deploy the trained surrogate, in conjunction with a large sample $X_M \sim p(\mathbf{x})$, to estimate α with each of the following methods:

- **hybMC ENT**: Our hybrid MC estimate (Eq. 7) where \mathcal{U} is chosen to contain the B points from X_M with highest entropy. [For now, ignore *hybMC ENT, we will return to it in Section 4.]
- **GP MC N** : Surrogate MC estimate (Eq. 4) using the surrogate trained on N points.
- **GP MC $N + B$** : Surrogate MC estimate (Eq. 4) using a surrogate trained on $N + B$ points.
- **hybMC CLOSE**: Inspired by Li and Xiu (2010), the hybrid MC estimate (Eq. 7) where \mathcal{U} is chosen to contain the B points from X_M which are predicted to be closest to the failure threshold (i.e., the samples with the smallest $|\mu_N(\mathbf{x}_i) - t|$).
- **SIIS**: Importance sampling estimate (Eq. 6; Peherstorfer et al., 2016) with a GMM bias distribution, also fit with the `Scikit-learn` package. The bias distribution is trained on the predicted failures, i.e., $\{\mathbf{x}_i \in X_M \mid \mu_N(\mathbf{x}_i) > t\}$.
- **SIIS UCB**: Same as SIIS, but the bias distribution is trained on the samples whose upper 90% confidence bound exceeds the threshold, i.e., $\{\mathbf{x}_i \in X_M \mid \mu_N(\mathbf{x}_i) + 1.645\sigma_N(\mathbf{x}_i) > t\}$.

Note, the first four methods are variations of Monte Carlo, and the last two are variations of importance sampling. Crucially, each method uses the exact same trained surrogate (besides GP MC $N + B$, which is trained further) and the exact same X_M sample. Differences in performance are thus attributed entirely to the estimation method. The GP MC N method is the only one which does not utilize the entire budget; it serves as a snapshot of the surrogate’s accuracy before it is combined with a hybrid calculation or importance sampling. We repeat each exercise 30 times with re-randomized starting designs.

To demonstrate functionality with a DGP, we additionally consider the 4d plateau function (Booth et al., 2024b). This function is known to be non-stationary; it is characterized by flat regions with a steep sloping drop between them. To address the complexity in the response surface, we use a Bayesian DGP surrogate (Sauer et al., 2023b) fit with the `deepgp` R-package (Booth, 2023). We train each DGP using

the contour location scheme of Booth et al. (2024b), which involves proposing triangulation candidates (Gramacy et al., 2022) and selecting the candidate on the Pareto front of entropy and uncertainty. To keep all of the code for this example in R for easy integration with the DGP, we leverage the `mclust` R-package (Scrucca et al., 2016) to train the GMM bias distribution. Given the increased complexity of the surrogate, we perform 20 re-randomized repetitions. Reproducible code for all experiments, including both the python and R implementations, is available in our public git repository.²

Results are shown in Figure 3, with true failure probability indicated by the red dashed line. The grey shaded region highlights the interval $\{\alpha \pm 2\sigma_\alpha\}$ where σ_α is calculated from the provided M . This region provides important context – it captures the intrinsic variability that would accompany any MC estimator. In other words, if we used the true simulator for all $\{\mathbf{x}_i\}_{i=1}^M$ samples (Eq. 2), we would obtain a boxplot roughly spanning the grey interval. We thus consider any results within this region to be effective estimates. We could tighten the interval (and the boxplots of the MC methods) by increasing M without requiring any additional simulator evaluations, another advantage MC holds over IS.

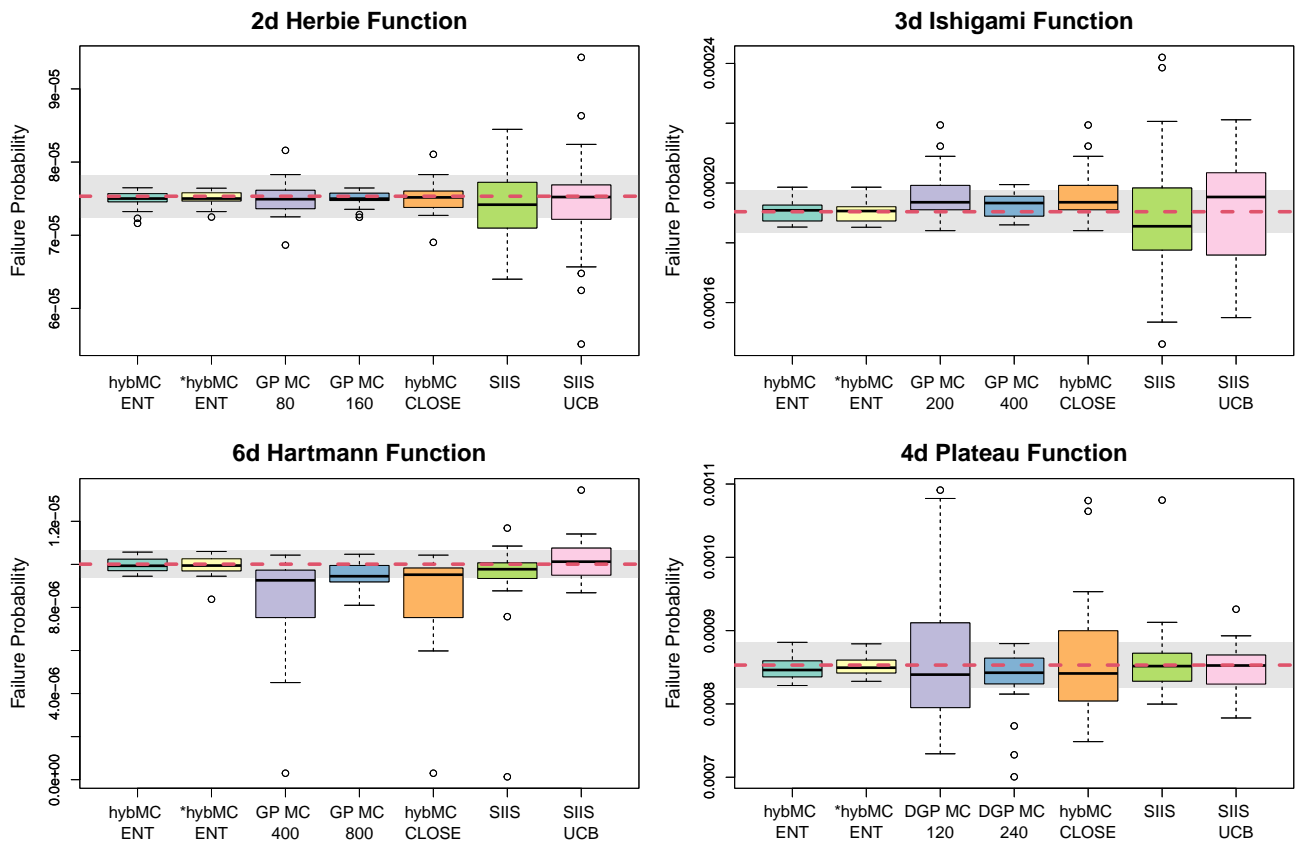


Figure 3: Estimated failure probabilities shown over true failure probability (red dashed) ± 2 standard errors (grey shading). Boxplots show 30 repetitions (20 for Plateau).

Our hybMC ENT method (teal) performed well across the board. Unsurprisingly, it was able to improve upon the accuracy of the original surrogate (purple) by leveraging the additional budget of B evaluations. More importantly, for all but the simplest Herbie function, it outperformed the surrogate MC estimates which made use of the full budget (blue). Recall, the (D)GP MC methods acquire points from \mathcal{X} , while the

²<https://bitbucket.org/boothlab/failprob/>

hybMC method acquires points from $p(\mathbf{x})$ (after the original training phase). The fact that hybMC is able to outperform the fully-trained surrogate indicates that at some point, it is better to prioritize expensive simulator evaluations for uncertain samples from $p(\mathbf{x})$ than to continue training the surrogate.

The strategy of Li and Xiu (2010) in allotting simulator evaluations based on predicted distance to the contour (hybMC CLOSE, orange) did not significantly improve upon the accuracy of the surrogate alone. This idea fails to leverage the UQ of the surrogate. It is possible for the surrogate to have higher uncertainty in its pass/fail prediction for a point further from the contour. For example, refer back to Figure 2. The entropy surrounding $x_1 = 1$ is far greater than that surrounding $x_1 = 0.5$, even though the latter of these is predicted to be closer to the contour (blue dashed line). Reserving true simulator evaluation for the $x_1 = 1$ location, where the surrogate would misclassify a failure, is preferable.

The SIIS methods (green and pink) had the poorest performance across the board. They particularly struggled in the simpler settings (Herbie and Ishigami), underperforming the simple GP MC N method which only used half the amount of simulator evaluations. We suspect the small budgets are to blame here; IS just needs more data, particularly when the GMM bias density is far from the ideal. Consequently, these IS variations had their best performance with the Hartmann function where 400 samples were budgeted for estimation. There appears to be very little benefit to the more conservative SIIS UCB (pink) over the traditional SIIS (green).

4 Allocating the simulation budget

Let $T = N + B$ represent the total budget of simulator evaluations, which is typically determined by the computational cost of the simulator. For expensive simulators which require long compute times, T may be only several hundred. We presume T is fixed, and we now address how to split it between N and B . In our previous studies, we evenly split T between training the surrogate and estimating α , i.e., $N = B = \frac{1}{2}T$. But this decision was admittedly arbitrary. In this section, we propose a scheme for allocating T between N and B , specifically for use within our hybrid Monte Carlo estimation scheme. Since the sum of N and B is fixed, this choice boils down to selecting N ; $B = T - N$ then follows directly. Ideally, we would like to halt training of the surrogate once learning has plateaued, saving the rest of the budget for the hybrid Monte Carlo estimate. If we stop training too early, the surrogate might be too inaccurate for the hybrid MC estimate to overcome. If we continue training for too long, we will not have any samples left for the hybrid estimation procedure. As we saw in Figure 3, in all but the simplest case, a MC estimate without any hybridization is suboptimal.

To monitor the surrogate’s learning, we propose tracking the progress of the surrogate MC estimate, $\hat{\alpha}_{\text{SURR}}$ (Eq. 4), which we will now denote as simply $\hat{\alpha}$. This estimator relies only on the trained surrogate and does not require additional simulator evaluations. As a demonstration, the left panel of Figure 4 reports the progress in $\hat{\alpha}$ for the 3d Ishigami function following the setup described in Section 3.2. To avoid excessive calculations, we evaluate the estimate after every 10th acquisition. It is apparent that the surrogate’s learning of the failure contour saturates well before it reaches $N = 200$, which we used in our previous experiments. The center panel of Figure 4 shows the relative difference between each successive $\hat{\alpha}$. As expected, the relative differences converge to zero as the surrogate hones in on the true contour, but they never settle at exactly zero (this is more apparent in the right panel which is zoomed in).

How small of an update then is small enough to indicate learning has plateaued? The significance of an update to $\hat{\alpha}$ is only interpretable within the context of α and M . Small differences might be inconsequential for large α with small M , but could be significant for small α with large M . To this end, we propose the use of the standard error σ_α to quantify the relative magnitude of each update. This standard error intrinsically accounts for the magnitude of α and M . Since the true α is unknown, we estimate $\hat{\sigma}_\alpha = \sqrt{\frac{\hat{\alpha}(1-\hat{\alpha})}{M}}$ using

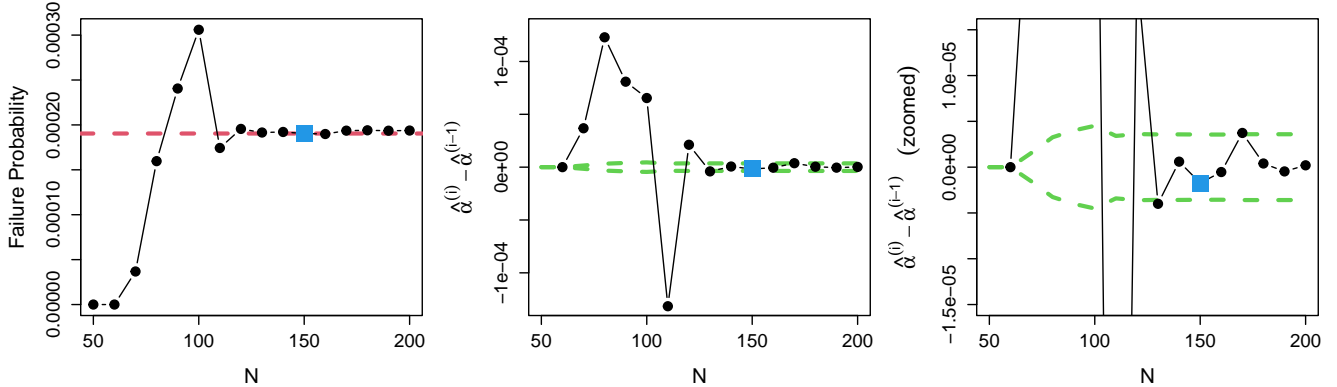


Figure 4: *Left*: Surrogate MC failure probability estimate for the Ishigami function, updated every 10th acquisition with true α in dashed red. *Center/Right*: Difference in successive estimates with $\pm\hat{\sigma}_\alpha$ shown in dashed green. The blue square marks the second update within $\pm\hat{\sigma}_\alpha$.

the current surrogate MC estimate. The green dashed lines in the center and right panels of Figure 5 show $\pm\hat{\sigma}_\alpha$ for the estimated failure probabilities. At the start, updates to $\hat{\alpha}$ are far beyond one standard error. But after a while, the updates sit comfortably within these bounds. We posit that, for a fixed sample X_M , any update to $\hat{\alpha}$ within $\pm\hat{\sigma}$ is “small enough.” Accordingly, we halt surrogate training once we have observed two successive updates within $\pm\hat{\sigma}$.

Our budgeting scheme is summarized as follows. Initialize a surrogate, begin a contour locating sequential design, and collect one sample X_M . At the start, it is likely that there will be no failures observed and that $\hat{\alpha}$ will be equal to zero (as is the case in Figure 4). To safeguard against halting surrogate training prematurely, we build in a “common sense” check by setting a minimum number of failures that must be observed before the contour location could be halted. If the contour location design is succeeding, it will be placing some points in the failure region. We recommend a default of 10 failures, but suggest increasing this for higher dimensional problems. In our synthetic experiments, we used a minimum of 10 failures for the Herbie, Ishigami, and plateau functions but bumped this up to 40 for the larger dimension of the Hartmann function. Once the surrogate has surpassed these minimum requirements, estimate $\hat{\alpha}$ after every 10th acquisition. Calculate $\hat{\sigma}_\alpha$ and check if $|\hat{\alpha}^{(\text{current})} - \hat{\alpha}^{(\text{previous})}| < \hat{\sigma}_\alpha$. Once this condition has been satisfied twice in a row, halt the sequential design and proceed to the hybrid Monte Carlo estimation following Section 3.1.

This stopping criterion requires the same X_M sample be used in every $\hat{\alpha}$ calculation. If a new X_M is generated for each estimate, there will naturally be more variability among the $\hat{\alpha}$ ’s, and the $\pm\hat{\sigma}_\alpha$ threshold would need to be increased. Removing this extraneous source of variability allows successive estimates to pinpoint differences stemming solely from the surrogate.

Revisiting synthetic experiments. We implemented this stopping criteria with each of the four functions described in Section 3.2. We used the same total budgets ($T = \{160, 400, 800, 240\}$, respectively), but chose N based on this decision rule. Once N was determined, we set $B = T - N$. All other simulation settings were the same. Figure 5 shows the distribution of chosen N values. The red star indicates the value used previously. Most repetitions halted surrogate training before the preset value, allotting more runs for estimation, but some proceeded longer. We view this variability as a strength – some random initializations need more data to effectively locate the contour while some get lucky from the start. Allowing the surrogate to dictate its own budget mitigates some of the risks of having an unlucky starting design.

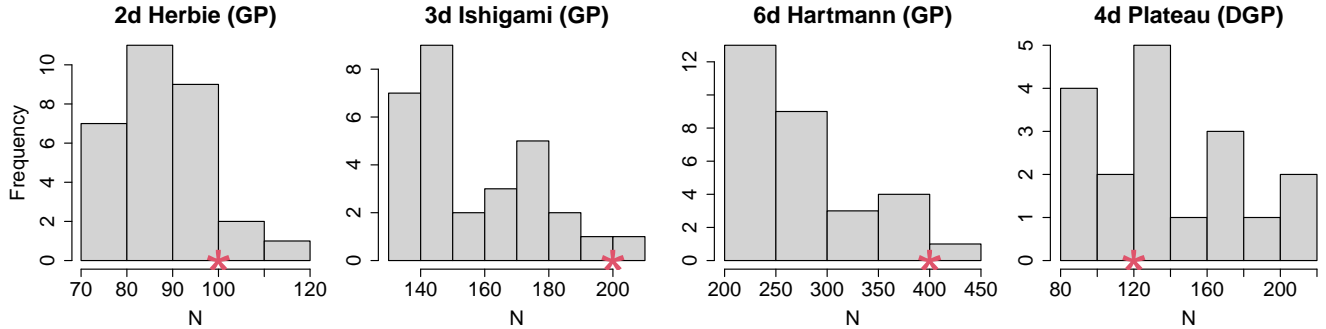


Figure 5: Distribution of the chosen N for each repetition of the synthetic examples from Figure 3. Red star indicates the value that was used previously.

The resulting failure probability estimates are shown as the *hybMC ENT method (yellow) in Figure 3. The original hybMC ENT methods already performed well, and we were able to match this performance with the budgeted *hybMC ENT method. We acknowledge the benefit of the budgeting method is not in beating the un-budgeted performance on synthetic problems, but in informing budget allocations in real-world scenarios when there is no clear choice for N and B .

5 RAE-2822 airfoil computer experiment

The RAE-2822 airfoil computer experiment simulates the flow of air around an aircraft wing. The simulation suite is solved via SU2, and the software is publicly available (Economou et al., 2016). The experiment accepts seven inputs: four shape parameters (S_i for $i = 1, \dots, 4$) and 3 environmental parameters, namely angle of attack, Reynolds number, and Mach number. We are interested in the lift over drag (L/D) ratio. L/D values that are too low represent inefficient flight conditions. We define a failure threshold at $t = 3$ such that $L/D < 3$ indicates failure. [Note the change from $f(\mathbf{x}) > t$ to $f(\mathbf{x}) < t$ does not affect the implementation of our method.] This computer experiment requires nearly 30 minutes of compute time with serial execution, but reductions are possible with parallel execution.

Our objective is to estimate the probability of failure given the following input distribution:

$$\begin{aligned}
 S_i &\sim \text{Unif}(-1e-4, 1e-4) \text{ for } i = 1, \dots, 4 \\
 \text{Angle of Attack} &\sim \mathcal{N}(\mu = 5, \sigma = 1) \text{ truncated to } [0, 10] \\
 \text{Reynolds number} &\sim \mathcal{N}(\mu = 1e7, \sigma = 1e6) \text{ truncated to } [5e6, 1.5e7] \\
 \text{Mach number} &\sim \mathcal{N}(\mu = 0.8, \sigma = 0.02) \text{ truncated to } [0.7, 0.9]
 \end{aligned}$$

We fix our total budget at $T = 500$ simulator evaluations. Booth et al. (2024b) found that DGP surrogates outperformed GP surrogates for contour location of this experiment. We follow the settings therein, starting with an LHS sample of size $n_0 = 100$ and fitting a Bayesian DGP surrogate with the `deepgp` package. We proceed with contour location following Booth et al. (2024b), stopping after every 10th acquisition to estimate $\hat{\alpha}$ and check whether it is within the $\pm\hat{\sigma}_\alpha$ bounds. Given the input dimension, we require at least 40 observed failures before we consider halting surrogate training. Since the true failure probability is unknown, we repeat this entire exercise with a newly randomized starting design for some additional context. Figure 6 reports the progress in $\hat{\alpha}$ over the course of each design.

Our stopping criterion halted the sequential designs at $N = 180$ and $N = 160$. For each repetition, we collect a separate random sample of size $M = 2.5 \times 10^6$, then identify the remaining points with the

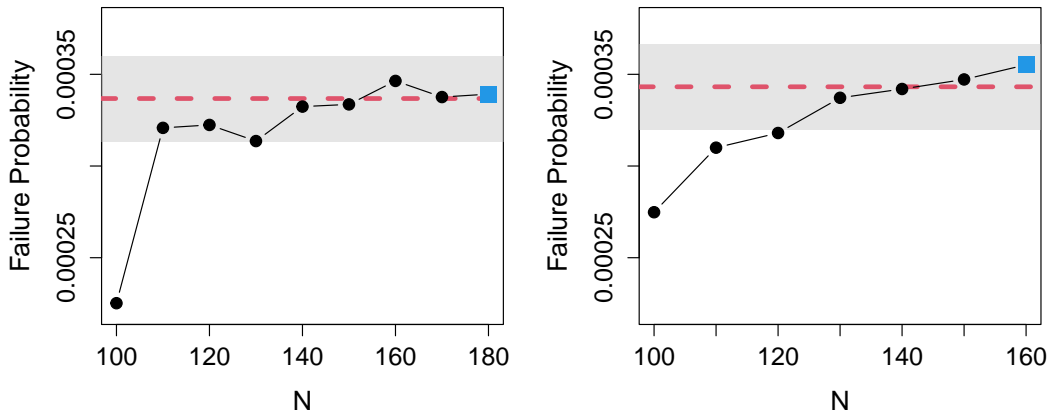


Figure 6: Two surrogate MC failure probability estimates for the airfoil computer experiment, updated every 10th acquisition with final estimates in dashed red. Grey shading indicates $\hat{\alpha} \pm \hat{\sigma}_\alpha$ for the final estimates.

highest entropy, and evaluate the true simulator at these locations. After updating the DGP surrogate, we obtain the final hybrid Monte Carlo estimates of $\hat{\alpha}_{\text{HYB}} = \{0.0003368, 0.0003432\}$, respectively. These values are indicated by the red dashed lines in Figure 6. The grey shading shows $\hat{\alpha} \pm \hat{\sigma}_\alpha$, calculated from these final hybrid estimates. Although the two estimates vary slightly, they are both within the bounds of reasonable variability for our chosen M . Additionally, notice how the final hybrid estimate of the second exercise (right panel) brought the failure probability lower than what the surrogate had estimated, closer to the estimate of our first attempt (left panel). We take this as an indication that the hybrid estimator is effectively adjusting for surrogate inaccuracies.

6 Discussion

We presented a hybrid Monte Carlo method for estimating failure probabilities of expensive computer experiments. Our hybrid method leverages the uncertainty quantification provided by a surrogate to reserve expensive simulator evaluations for samples with high classification uncertainty. We limited our experiments to GP and DGP surrogates, but our proposed estimator is applicable to any surrogate which provides posterior predictive distributions (required for calculation of entropy). Extensions to other surrogates, such as treed Gaussian processes (Gramacy and Lee, 2008) or Bayesian additive regression trees (Chipman et al., 2010), is straightforward.

Our hybrid MC estimator is computationally efficient in the number of evaluations of the expensive simulator, but it requires many predictive evaluations from the surrogate. Posterior predictions must be gathered at all M sample points. While surrogate predictions are very cheap, collecting millions of them is not necessarily trivial. Our experiments were limited to failure probabilities above 1×10^{-5} for this very reason. We could tackle smaller failure probabilities, but it would require larger M , which would eventually become impractical. Our approach may simply not be suited to very rare failure probabilities.

The efficacy of any surrogate-informed failure probability estimation relies on the surrogate’s ability to accurately classify failures. Although our hybrid estimator is generally applicable, we strongly recommend the use of contour locating sequential designs to train the surrogate. We proposed a budgeting scheme which informs allocation of simulator evaluations between surrogate training and failure probability estimation

based on progress in the surrogate Monte Carlo estimate. If a budget is severely restricted, the budget could be exhausted training the surrogate before our proposed stopping criterion is met. While this is not ideal, we contend that fully-training a surrogate and using a surrogate MC estimate is the best option in this scenario. Particularly in light of the data hungry nature of IS-based methods, which perform poorly in small data settings.

When the input distribution is not uniform over \mathcal{X} , it could be beneficial to leverage information about $p(\mathbf{x})$ in the sequential training of the surrogate (Abdelmalek-Lomenech et al., 2024). There is arguably no need to train a surrogate in a region where inputs will not plausibly occur, such as in the outer corners of the Herbie function surface (Figure 1, center). Incorporating this information in the contour location stage could improve failure probability estimation downstream. But in the case of rare probabilities, it may be hard to draw the line between regions that are plausible and ones that are not. This avenue is currently underexplored.

References

- Abdelmalek-Lomenech, R. A., Bect, J., Chabridon, V., and Vazquez, E. (2024). “Bayesian sequential design of computer experiments for quantile set inversion.” *Technometrics*, , just-accepted, 1–14.
- Azzimonti, D., Ginsbourger, D., Chevalier, C., Bect, J., and Richet, Y. (2021). “Adaptive design of experiments for conservative estimation of excursion sets.” *Technometrics*, 63, 1, 13–26.
- Batet, L., Alvarez-Fernandez, J. M., de les Valls, E. M., Martinez-Quiroga, V., Perez, M., Reventos, F., and Sedano, L. (2014). “Modelling of a supercritical CO2 power cycle for nuclear fusion reactors using RELAP5–3D.” *Fusion Engineering and Design*, 89, 4, 354–359.
- Bect, J., Ginsbourger, D., Li, L., Picheny, V., and Vazquez, E. (2012). “Sequential design of computer experiments for the estimation of a probability of failure.” *Statistics and Computing*, 22, 773–793.
- Belot, I., Vidal, D., Greiner, R., Votsmeier, M., Hayes, R. E., and Bertrand, F. (2021). “Impact of washcoat distribution on the catalytic performance of gasoline particulate filters as predicted by lattice Boltzmann simulations.” *Chemical Engineering Journal*, 406, 127040.
- Bichon, B. J., Eldred, M. S., Swiler, L. P., Mahadevan, S., and McFarland, J. M. (2008). “Efficient global reliability analysis for nonlinear implicit performance functions.” *AIAA journal*, 46, 10, 2459–2468.
- Booth, A. S. (2023). *deepgp: Bayesian Deep Gaussian Processes using MCMC*. R package version 1.1.3.
- Booth, A. S., Gramacy, R., and Renganathan, A. (2024a). “Actively learning deep Gaussian process models for failure contour and probability estimation.” In *AIAA SCITECH 2024 Forum*, 0577.
- Booth, A. S., Renganathan, S. A., and Gramacy, R. B. (2024b). “Contour Location for Reliability in Airfoil Simulation Experiments using Deep Gaussian Processes.” *Annals of Applied Statistics*, , just-accepted. ArXiv:2308.04420.
- Bugallo, M. F., Elvira, V., Martino, L., Luengo, D., Miguez, J., and Djuric, P. M. (2017). “Adaptive importance sampling: The past, the present, and the future.” *IEEE Signal Processing Magazine*, 34, 4, 60–79.
- Cheng, K. and Lu, Z. (2020). “Structural reliability analysis based on ensemble learning of surrogate models.” *Structural Safety*, 83, 101905.

- Cheng, K., Papaioannou, I., Lu, Z., Zhang, X., and Wang, Y. (2023). “Rare event estimation with sequential directional importance sampling.” *Structural Safety*, 100, 102291.
- Chevalier, C., Bect, J., Ginsbourger, D., Vazquez, E., Picheny, V., and Richet, Y. (2014). “Fast parallel kriging-based stepwise uncertainty reduction with application to the identification of an excursion set.” *Technometrics*, 56, 4, 455–465.
- Chipman, H. A., George, E. I., and McCulloch, R. E. (2010). “BART: Bayesian additive regression trees.” *The Annals of Applied Statistics*, 4, 1, 266 – 298.
- Cole, D. A., Gramacy, R. B., Warner, J. E., Bomarito, G. F., Leser, P. E., and Leser, W. P. (2023). “Entropy-based adaptive design for contour finding and estimating reliability.” *Journal of Quality Technology*, 55, 1, 43–60.
- Dalbey, K. R. and Swiler, L. P. (2014). “Gaussian process adaptive importance sampling.” *International Journal for Uncertainty Quantification*, 4, 2.
- Damianou, A. and Lawrence, N. D. (2013). “Deep gaussian processes.” In *Artificial intelligence and statistics*, 207–215. PMLR.
- Duhamel, C., Helbert, C., Munoz Zuniga, M., Prieur, C., and Sinoquet, D. (2023). “A SUR version of the Bichon criterion for excursion set estimation.” *Statistics and Computing*, 33, 2, 41.
- Echard, B., Gayton, N., and Lemaire, M. (2011). “AK-MCS: an active learning reliability method combining Kriging and Monte Carlo simulation.” *Structural Safety*, 33, 2, 145–154.
- Economon, T. D., Palacios, F., Copeland, S. R., Lukaczyk, T. W., and Alonso, J. J. (2016). “SU2: An open-source suite for multiphysics simulation and design.” *Aiaa Journal*, 54, 3, 828–846.
- Gramacy, R. B. (2020). *Surrogates: Gaussian process modeling, design, and optimization for the applied sciences*. CRC press.
- Gramacy, R. B. and Apley, D. W. (2015). “Local Gaussian process approximation for large computer experiments.” *Journal of Computational and Graphical Statistics*, 24, 2, 561–578.
- Gramacy, R. B. and Lee, H. K. H. (2008). “Bayesian treed Gaussian process models with an application to computer modeling.” *Journal of the American Statistical Association*, 103, 483, 1119–1130.
- Gramacy, R. B., Sauer, A., and Wycoff, N. (2022). “Triangulation candidates for bayesian optimization.” *Advances in Neural Information Processing Systems*, 35, 35933–35945.
- Haldar, A. and Mahadevan, S. (1995). “First-order and second-order reliability methods.” In *Probabilistic Structural Mechanics Handbook: theory and industrial applications*, 27–52. Springer.
- Hristov, P., DiazDelaO, F., Farooq, U., and Kubiak, K. (2019). “Adaptive Gaussian process emulators for efficient reliability analysis.” *Applied Mathematical Modelling*, 71, 138–151.
- Ishigami, T. and Homma, T. (1990). “An importance quantification technique in uncertainty analysis for computer models.” In *[1990] Proceedings. First international symposium on uncertainty modeling and analysis*, 398–403. IEEE.
- Joseph, V. R. (2016). “Space-filling designs for computer experiments: A review.” *Quality Engineering*, 28, 1, 28–35.

- Kurtz, N. and Song, J. (2013). “Cross-entropy-based adaptive importance sampling using Gaussian mixture.” *Structural Safety*, 42, 35–44.
- Lee, H., Gramacy, R., Linkletter, C., and Gray, G. (2011). “Optimization subject to hidden constraints via statistical emulation.” *Pacific Journal of Optimization*, 7, 3, 467–478.
- Li, J. and Xiu, D. (2010). “Evaluation of failure probability via surrogate models.” *Journal of Computational Physics*, 229, 23, 8966–8980.
- Li, M., Wang, G., Qian, L., Li, X., and Ma, Z. (2021). “ASS-GPR: Adaptive Sequential Sampling Method Based on Gaussian Process Regression for Reliability Analysis of Complex Geotechnical Engineering.” *International Journal of Geomechanics*, 21, 10, 04021192.
- Lu, N., Li, Y.-F., Huang, H.-Z., Mi, J., and Niazi, S. G. (2023). “AGP-MCS+ D: An active learning reliability analysis method combining dependent Gaussian process and Monte Carlo simulation.” *Reliability Engineering & System Safety*, 240, 109541.
- MacKay, D. J. (1995). “Bayesian neural networks and density networks.” *Nuclear Instruments and Methods in Physics Research Section A: Accelerators, Spectrometers, Detectors and Associated Equipment*, 354, 1, 73–80.
- Marques, A., Lam, R., and Willcox, K. (2018). “Contour location via entropy reduction leveraging multiple information sources.” *Advances in neural information processing systems*, 31.
- McKay, M. D., Beckman, R. J., and Conover, W. J. (2000). “A comparison of three methods for selecting values of input variables in the analysis of output from a computer code.” *Technometrics*, 42, 1, 55–61.
- Mia, M. S., Islam, M. S., and Ghosh, U. (2017). “Modal analysis of cracked cantilever beam by finite element simulation.” *Procedia engineering*, 194, 509–516.
- Ming, D., Williamson, D., and Guillas, S. (2023). “Deep Gaussian process emulation using stochastic imputation.” *Technometrics*, 65, 2, 150–161.
- Oh, M.-S. and Berger, J. O. (1992). “Adaptive importance sampling in Monte Carlo integration.” *Journal of statistical computation and simulation*, 41, 3-4, 143–168.
- O’Hagan, A. (1987). “Monte Carlo is fundamentally unsound.” *The Statistician*, 247–249.
- Park, C., Haftka, R. T., and Kim, N. H. (2017). “Remarks on multi-fidelity surrogates.” *Structural and Multidisciplinary Optimization*, 55, 1029–1050.
- Pedregosa, F., Varoquaux, G., Gramfort, A., Michel, V., Thirion, B., Grisel, O., Blondel, M., Prettenhofer, P., Weiss, R., Dubourg, V., et al. (2011). “Scikit-learn: Machine learning in Python.” *the Journal of machine Learning research*, 12, 2825–2830.
- Peherstorfer, B., Cui, T., Marzouk, Y., and Willcox, K. (2016). “Multifidelity importance sampling.” *Computer Methods in Applied Mechanics and Engineering*, 300, 490–509.
- Picheny, V., Wagner, T., and Ginsbourger, D. (2013). “A benchmark of kriging-based infill criteria for noisy optimization.” *Structural and multidisciplinary optimization*, 48, 607–626.

- Rajaram, D., Puranik, T. G., Ashwin Renganathan, S., Sung, W., Fischer, O. P., Mavris, D. N., and Ramamurthy, A. (2021). “Empirical assessment of deep gaussian process surrogate models for engineering problems.” *Journal of Aircraft*, 58, 1, 182–196.
- Ranjan, P., Bingham, D., and Michailidis, G. (2008). “Sequential experiment design for contour estimation from complex computer codes.” *Technometrics*, 50, 4, 527–541.
- Rasmussen, C. E., Williams, C. K., et al. (2006). *Gaussian processes for machine learning*, vol. 1. Springer.
- Renganathan, A. (2024). “Efficient reliability analysis with multifidelity Gaussian processes and normalizing flows.” In *AIAA SCITECH 2024 Forum*, 0576.
- Renganathan, S. A., Rao, V., and Navon, I. M. (2023). “CAMERA: A method for cost-aware, adaptive, multifidelity, efficient reliability analysis.” *Journal of Computational Physics*, 472, 111698.
- Reynolds, D. A. et al. (2009). “Gaussian mixture models.” *Encyclopedia of biometrics*, 741, 659-663.
- Santner, T. J., Williams, B. J., Notz, W. I., and Williams, B. J. (2003). *The design and analysis of computer experiments*, vol. 1. Springer.
- Sauer, A. (2023). “Deep Gaussian process surrogates for computer experiments.” Ph.D. thesis, Virginia Polytechnic Institute and State University.
- Sauer, A., Cooper, A., and Gramacy, R. B. (2023a). “Vecchia-approximated deep Gaussian processes for computer experiments.” *Journal of Computational and Graphical Statistics*, 32, 3, 824–837.
- Sauer, A., Gramacy, R. B., and Higdon, D. (2023b). “Active learning for deep Gaussian process surrogates.” *Technometrics*, 65, 4–18.
- Scrucca, L., Fop, M., Murphy, T. B., and Raftery, A. E. (2016). “mclust 5: clustering, classification and density estimation using Gaussian finite mixture models.” *The R Journal*, 8, 1, 289–317.
- Srinivasan, R. (2002). *Importance sampling: Applications in communications and detection*. Springer Science & Business Media.
- Su, G., Peng, L., and Hu, L. (2017). “A Gaussian process-based dynamic surrogate model for complex engineering structural reliability analysis.” *Structural Safety*, 68, 97–109.
- Tabandeh, A., Jia, G., and Gardoni, P. (2022). “A review and assessment of importance sampling methods for reliability analysis.” *Structural Safety*, 97, 102216.
- Tokdar, S. T. and Kass, R. E. (2010). “Importance sampling: a review.” *Wiley Interdisciplinary Reviews: Computational Statistics*, 2, 1, 54–60.
- Yazdi, F. (2022). “Fast deep gaussian process modeling and design for large complex computer experiments.” Ph.D. thesis, Simon Fraser University.

SUPPLEMENTARY MATERIAL

Here we provide the details of the functions, thresholds, and input distributions used in the benchmark exercises of Section 3.2. In each case, failures are defined as $f(\mathbf{x}) > t$.

Herbie. The 2d Herbie function (Lee et al., 2011) is defined in over $[-2, 2]^2$ as

$$f(\mathbf{x}) = \prod_{i=1}^2 \exp(-(x_i - 1)^2) + \exp(-0.8 * (x_i + 1)^2) - 0.05 * \sin(8 * (x_i + 1)).$$

We set the failure threshold at $t = 1.065$ and define the input distribution as $x_i \stackrel{\text{ind}}{\sim} \mathcal{N}(0, 0.36)$ for $i = 1, 2$, truncated to $[-2, 2]$.

Ishigami. The 3d Ishigami function (Ishigami and Homma, 1990) is defined over $[-\pi, \pi]^3$ as

$$f(\mathbf{x}) = \sin(x_1) + 5 * \sin(x_2)^2 + 0.1 * x_3^4 * \sin(x_1).$$

We set the failure threshold at $t = 10.244$ and define the input distribution as

$$\begin{aligned} x_1 &\sim \mathcal{N}(-1, 1) \text{ truncated to } [-\pi, \pi] \\ x_2 &\sim \mathcal{N}(1.5, 1.5) \text{ truncated to } [-\pi, \pi] \\ x_3 &\sim \text{Uniform}(-\pi, \pi). \end{aligned}$$

Hartmann. The 6d Hartmann function (Picheny et al., 2013) is defined over $[0, 1]^6$ as

$$f(\mathbf{x}) = - \sum_{i=1}^4 \alpha_i \exp \left(- \sum_{j=1}^6 A_{ij} (x_j - P_{ij})^2 \right) \text{ where}$$

$$\alpha^\top = \begin{bmatrix} 1 \\ 1.2 \\ 3 \\ 3.2 \end{bmatrix} \quad A^\top = \begin{bmatrix} 10 & .05 & 3 & 17 \\ 3 & 10 & 3.5 & 8 \\ 17 & 17 & 1.7 & .05 \\ 3.5 & .1 & 10 & 10 \\ 7 & 8 & 17 & .1 \\ 8 & 14 & 8 & 14 \end{bmatrix} \quad \text{and} \quad P^\top = \begin{bmatrix} .1312 & .2329 & .2348 & .4047 \\ .1696 & .4135 & .1451 & .8828 \\ .5569 & .8307 & .3522 & .8732 \\ .0124 & .3736 & .2883 & .5743 \\ .8283 & .1004 & .3047 & .1091 \\ .5886 & .9991 & .6650 & .0381 \end{bmatrix}.$$

We set the failure threshold at $t = 2.46$ and define the input distribution as $x_i \stackrel{\text{ind}}{\sim} \mathcal{N}(0.5, 0.1)$ for $i = 1, \dots, 6$, truncated to $[0, 1]$.

Plateau. The Plateau function (Booth et al., 2024b) is defined in arbitrary dimension over $[0, 1]^d$ as

$$f(\mathbf{x}) = 2 * \Phi \left[\sqrt{2} \left(-4 - 3 \sum_{i=1}^3 (4x_i - 2) \right) \right] - 1$$

where Φ is the standard Gaussian CDF. We use $d = 4$ and set the failure threshold at $t = 0$. We define the input distribution as $x_i \stackrel{\text{ind}}{\sim} \mathcal{N}(0.5, 0.085)$ for $i = 1, \dots, 4$, truncated to $[0, 1]$.